

Electronic structure of the shallow boron acceptor in 6H-SiC: A pulsed EPR/ENDOR study at 95 GHz

T. Matsumoto, O. G. Poluektov, and J. Schmidt

Huygens Laboratory, Leiden University, P.O. Box 9504, 2300 RA Leiden, The Netherlands

E. N. Mokhov and P. G. Baranov

A. F. Ioffe Physico-Technical Institute, Politechnicheskaya 26, 194021 St. Petersburg, Russia

(Received 5 August 1996)

A high-frequency pulsed electron paramagnetic resonance electron-nuclear double-resonance (ENDOR) study on a ^{13}C -enriched 6H-SiC single crystal is reported. This type of spectroscopy, owing to its superior spectral resolution, allows us to obtain detailed information about the electronic structure of the shallow boron acceptor centers in 6H-SiC. It is concluded that around 40% of the spin density is localized in the p_z orbital of a carbon which is nearest to boron. The p_z orbital is directed along the C-B connection line and is parallel to the c axis for the hexagonal site and 70° away from the c axis for the two quasicubic sites. We conclude that the C-B bond is a dangling bond, that boron is neutral, and that there is no direct spin density on boron. There is a relaxation of the carbon atom, carrying the spin density, and the boron atom away from each other. From a ^{29}Si and ^{13}C ENDOR study it is further concluded that around 60% of the spin density is distributed in the crystal with a Bohr radius of 2.2 Å. [S0163-1829(97)04603-1]

I. INTRODUCTION

Boron is the most important shallow acceptor in SiC, and its electronic structure has been studied intensively by electron paramagnetic resonance (EPR) spectroscopy,¹⁻¹⁶ since the first paper by Woodbury and Ludwig in 1961.¹ The structure of the shallow boron acceptor has been reinterpreted several times, and several contradictory models have been proposed. After the first publication, it was believed for a long time that boron substitutes for carbon, as only superhyperfine (hf) interaction with ^{29}Si was observed. It was established that boron in the 6H-SiC crystal occupies three different sites with equal probability: two quasicubic (k_1 and k_2) sites and one hexagonal (hex) site.

In 1986 Zubatov *et al.*⁵ published the results of EPR experiments on a ^{13}C -enriched 6H-SiC crystal, and reported a large anisotropic hf interaction with one ^{13}C nucleus. In their model boron occupies a silicon position, with the main spin density located on the dangling bond of a carbon atom along the C-B connection line. The observed super hf interaction with ^{29}Si was attributed to the three silicon atoms near the carbon with the maximum spin density.

The remarkable aspect of the boron acceptor is that its g tensor hardly shows an anisotropy (the average $g \approx 2$). This is in stark contrast to the aluminum and gallium shallow acceptors.⁶⁻⁸ Here the g tensors are very anisotropic, with values that are in good agreement with predictions based on effective-mass theory. This difference in behavior was explained by considering the differences in the atomic radii. It was proposed that boron and beryllium, with atomic radii smaller than silicon, occupy off-center positions, i.e., they relax away from the neighboring carbon along the C-B (Be) bond.⁹ Such a displacement of carbon along the C-B bond was already suggested in Ref. 5. A similar displacement for Boron in the hexagonal site in 6H-SiC was proposed in Ref. 10; and in 3C-SiC in Refs. 11 and 12. In contrast, aluminum

and gallium, with atomic radii larger than silicon, substitute for silicon and do not undergo a displacement. As a result, for boron and beryllium the orbital angular momentum of the hole is quenched and $g \approx 2$. In contrast, for aluminum and gallium the orbital angular momentum is conserved, and the hole reflects the properties of the valence band.

In more recent publications a description of the shallow boron acceptor was given on the basis of electron-nuclear double-resonance (ENDOR) and optical detection of magnetic resonance (ODMR) investigations.¹³⁻¹⁶ In this model the valence electron of a neighboring carbon is donated to boron, thus forming a $B_{\text{Si}}^- - C^+$ bond. The unpaired electron of C^+ is uniformly distributed among the three remaining bonding orbitals, and boron and carbon relax toward each other. The authors call this model the "boron-induced carbon acceptor."

The presence of two alternative models was a motivation for us to perform an experiment, from which the electronic and geometric structure of the boron acceptor in SiC can be unambiguously determined. In this contribution we present the results of a high-frequency (95 GHz) EPR and ENDOR study of the shallow boron acceptor in a ^{13}C -enriched 6H-SiC crystal. The high spectral resolution of this technique allows us to resolve all magnetically inequivalent boron sites and to measure accurately their g tensor. Moreover, we obtained the hyperfine tensors of the nuclear spin of ^{11}B and the nuclear spin of ^{13}C of the neighboring carbon atom for each site. The results allow us to present a consistent model for the electronic structure of the shallow boron acceptor in 6H-SiC which explains all magnetic resonance data. We conclude that the main spin density of the unpaired electron is located on the p orbital of carbon along the B-C connection line as originally suggested by Zubatov *et al.*⁵ There is no spin density on boron, which has a neutral charge, and the carbon and boron atoms are shifted away from each other. From a ^{29}Si and ^{13}C ENDOR study it is further concluded that about 60% of the spin density is distributed in the crystal

with a Bohr radius of 2.2 \AA , a value which is in reasonable agreement with effective-mass theory.

II. EXPERIMENT

The samples, used in the experiment, were free-standing epitaxial layers (with removed substrates) compensated with ^{11}B during diffusion. The epitaxial layers were grown by the sublimation sandwich method¹⁷ in vacuum at temperatures between 1700 and 1750 °C. As grown, the epitaxial layers were n type, owing to nitrogen donors. Boron was diffused at a temperature of about 2000 °C. Two types of samples were studied: ^{13}C -enriched crystals of 6H-SiC and crystals with a natural isotopic abundance of carbon.

The experiments were performed on a home-built, high-frequency, pulsed EPR/ENDOR spectrometer operating at a microwave frequency of 95 GHz. A detailed description of the setup is given elsewhere.^{18,19} The main advantage of the high-frequency spectrometer is the high resolution both in the EPR and ENDOR spectra. Moreover, owing to a split-coil configuration of the superconducting magnet, it is possible to perform a complete orientational study. In the pulsed ENDOR experiment a Mims-type pulse sequence was used.²⁰ The separation between the first and second microwave pulse was varied from 200 to 700 ns, and between the second and third pulse from 0.4 to 1 ms. The radio frequency pulse was applied between the last two microwave pulses. Low-temperature measurements were done at 1.5 K. For the temperature-dependent experiments the temperature was stabilized with a helium gas flow with an accuracy of ± 1 K.

III. RESULTS

A. Angular dependence of the EPR spectra

The angular dependence of the 95-GHz EPR spectra at 1.5 K of the shallow boron acceptor in 6H-SiC is almost the same as the one reported by Zubatov *et al.*⁵ at 4.2 K, but differs from that of Reinke *et al.*¹⁵ at 1.5 K. However, our conclusions concerning the g tensors of the various sites differ from the assignments of these two research groups, and since the g values are important parameters for our discussion, we review the results and the analysis of the EPR data in this section.

The direction of the principal z axis of the g tensors of three species were found as extreme positions in the angular dependence of the EPR spectra in the high-magnetic-field region. The accuracy of the positions of these extrema is $\pm 1^\circ$, and is limited by the widths of the EPR lines and the steepness of their orientational dependences. We note that the W -band EPR lines are slightly broader than those recorded at the X band, and also that the hyperfine structure caused by the boron nuclear spin is hardly visible. This effect is partially caused by g strain, which is often observed to some extent for species with anisotropic g tensors, and partially by super hf interaction with ^{13}C nuclei.

In agreement with previous reports, three types of centers were observed in the EPR spectra. One (called B_3 in Ref. 5) has axial symmetry with $g_z \parallel c$. The other two are found with their g_z axes directed along the six equivalent orientations within the hexagonal crystal lattice. They are nearly axial about their g_z axes, which are 110° (or 70°) away from the c

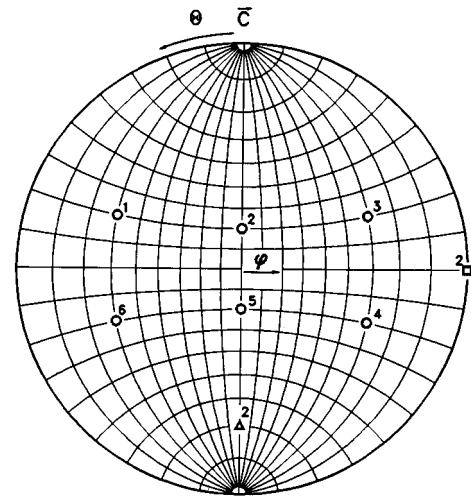


FIG. 1. The Wulff net projection of the directions of the g_z principal axes of the B_1 and B_2 centers in 6H-SiC (open circles). For magnetic subsite 2 the direction of the principal g_x axis is indicated by a square and the direction of g_y by a triangle.

axis. They correspond to the centers B_1 and B_2 of Ref. 5. Note however that in Ref. 5 the smallest g values are assigned to g_x , whereas in our case they are assigned to g_z . The one with the smaller g_z value will be called B_1 and the other B_2 . The directions of these g_z axes are indicated by circles in the Wulff net projection in Fig. 1. The directions of the g_x and g_y axes were found as low-magnetic-field extrema or turning points 90° away from the corresponding g_z extremum. They are shown with a square and a triangle for the center indicated by 2 in Fig. 1. Here, we introduce two angles θ and ϕ to describe the directions: θ is the azimuthal angle from the c axis, and ϕ is the longitudinal angle around the c axis with its origin defined by the direction of the g_z axis for B_1 or B_2 centers in one of the six orientations.

Angular Dependence of EPR

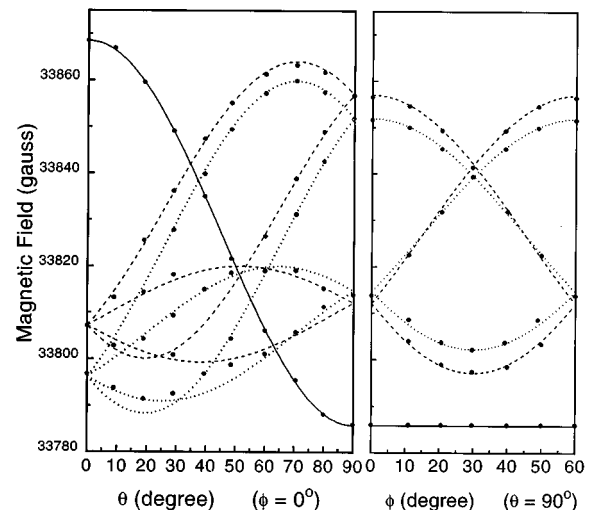


FIG. 2. The orientational dependences of the EPR lines of the shallow boron acceptor in 6H-SiC. Points indicate the position of the main peaks in the EPR spectra. Solid lines are calculated curves for center B_3 , broken lines for center B_1 , and the dotted line for center B_2 . $T=1.2$ K.

TABLE I. The principal value of the g tensor of the shallow boron acceptor in 6H-SiC for the different sites k_1 , k_2 , and hex.

	Present results			Zubatov <i>et al.</i> (Ref. 5)		
	g_x	g_y	g_z	g_x	g_y	g_z
$B_1 (k_1)$	2.006 23	2.006 05	2.002 26	2.0021	2.0062	2.0059
$B_2 (k_2)$	2.005 92	2.006 75	2.002 51	2.0028	2.0059	2.0062
B_3 (hex)	2.006 90	2.006 80	2.002 00	2.0068	2.0069	2.0020
			$\pm 0.000 05$			± 0.0005

In Fig. 2 the orientational dependence of the EPR lines is shown. Points indicate the positions of the main peaks in the EPR spectra. Solid lines are calculated curves for center B_3 , broken and dotted lines for centers B_1 and B_2 , which consist of six orientationally inequivalent sites. The parameters used in the calculation are given in Table I. The directions of the g_y axes of B_1 and B_2 are in a plane spanned by the c axes and their g_z axes, whereas their g_x axes are perpendicular to this plane. All g_x extrema are in the plane perpendicular to the c axis. Thus, for example, as can be seen in Fig. 1, for a center B_1 or B_2 with its g_z axis in the direction $\theta=110^\circ$, $\phi=0^\circ$, the g_y axis is in the direction $\theta=20^\circ$, $\phi=0^\circ$, and the g_x axis is in the direction $\theta=90^\circ$, $\phi=90^\circ$. Relative Δg values of the g -tensor were measured with a high accuracy of $\pm 0.000 05$, and were limited by the width of the EPR lines. The absolute accuracy of the g values is lower, and amounts to ± 0.0002 . For this reason, we fix the g_z value of the B_3 center with $\mathbf{B} \parallel c$ equal to 2.0020. This seems to be the most reliable parameter, since the same value has been reported by several authors.^{1,3,5,15} A good overall agreement has been obtained between the experimental points and the calculated curves. The relatively poor fit observed in the magnetic-field region 3.3790~3.3820 T is due to broadening and overlapping of the EPR peaks of the 12 orientationally inequivalent sites of the B_1 and B_2 centers. In order to optimize the accu-

racy of the determined g values, EPR spectra for different orientations of the magnetic field were simulated taking into account the hf interaction with ^{11}B (see below).

In Fig. 3 the experimental EPR spectra and simulations are shown. The simulation was done using the g values in Table I and the hf parameters in Table II, which were obtained from ENDOR measurements. A Lorentzian line shape was assumed for each EPR line. We slightly adjusted the widths (2.0 ± 0.4 G) and intensity ratio of the EPR lines of the different centers from spectrum to spectrum, because they depend on the width and separation of the microwave pulses. The shape of the experimental curves, including the region of 3.3790~3.3820 T, where many lines overlap, are well reproduced by the simulation. The perfect agreement between experimental and simulated spectra supports the assignment of the g tensors. Small changes in the simulation parameters, by 0.000 05 for the g values and by 2° for the orientation of the principal axes of the g tensors, completely destroys the agreement between experiment and simulation.

Upon closer inspection, one can find some weak lines or shoulders in the experimental curves which are not reproduced in the simulations. They are caused by hf interactions with nuclei other than ^{11}B , such as ^{29}Si and ^{13}C which were not taken into account in the simulation, and by the signal from the nitrogen donor, which appears around 3.3835 T at

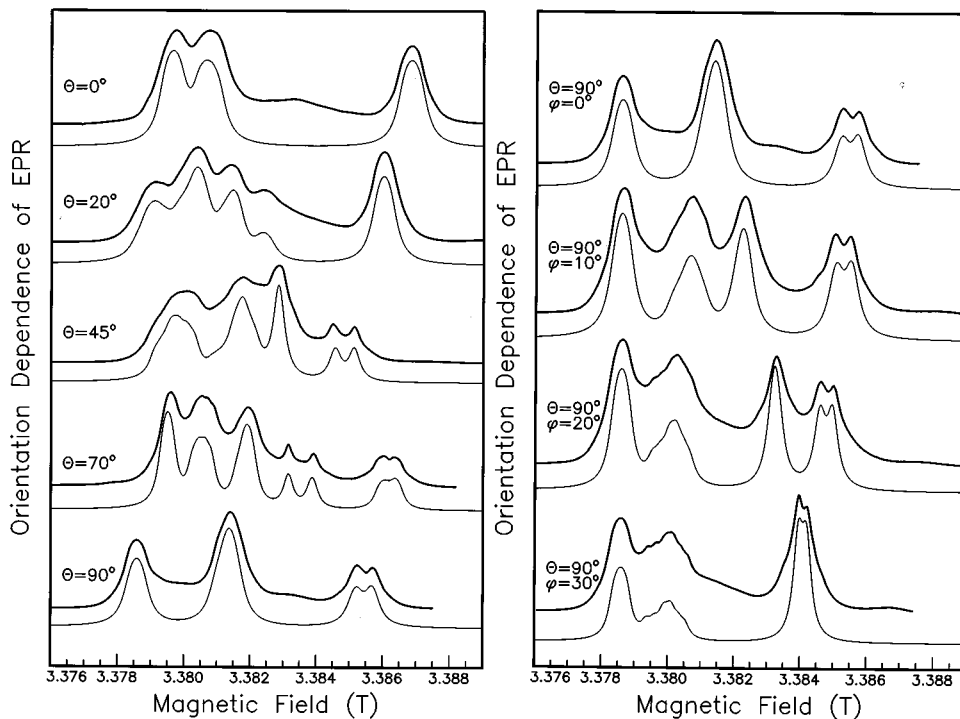


FIG. 3. The experimental (thick lines) and simulated (thin lines) EPR spectra of 6H-SiC:B for different orientations of the magnetic field. The angles θ and ϕ define the orientation of the magnetic field with respect to the crystal axes. For definitions, see the text.

TABLE II. The hf and quadrupole parameters for ^{11}B . The directions of the principal axes coincide within $\pm 2^\circ$ with the principal axes of the g tensor. a , b , and q are related to the tensor elements of A and Q as follows: $A_{zz} = a + 2b$, $A_{yy} = a - b$, and $Q_{zz} = 2q$. The signs of the parameters from Ref. 13 are given here in accordance with Ref. 16.

	This study			Refs. 10 and 13		
	a (MHz) ± 0.05	b (MHz) ± 0.05	q (kHz) ± 5	a (MHz)	b (MHz)	q (kHz)
B_1 (k_1)	-3.72	3.06	255	2.893	-2.786	248
B_2 (k_2)	-2.99	2.89	250	3.828	-3.031	243
B_3 (hex)	-0.97	2.91	242	0.973	-2.981	251

$\theta=0^\circ$. Shoulders are seen in the EPR spectrum of Fig. 3, on both sides of the highest field peak ($\theta=90^\circ$, $\phi=30^\circ$) in the spectrum. They are more clearly recognized in the derivative spectrum in Fig. 4. Two pairs of shoulders with their central positions coinciding with the main peaks of B_1 and B_2 are seen. They correspond to the ^{29}Si ($I=\frac{1}{2}$, abundance 4.7%) super hf lines, reported in the previous papers,^{1,5} and can also be clearly seen in a ^{13}C nonenriched SiC sample. The hf splitting was found to be almost isotropic with $a=10\times 10^{-4}$ T and $b<1\times 10^{-4}$ T, in agreement with Ref. 5.

In the ^{13}C -enriched sample, additional EPR lines are observed, which are not present in a ^{13}C nonenriched SiC sample. For example, the line at 3.3875 T in the $\theta=90^\circ$, $\phi=20^\circ$ spectrum, which has also been observed by Zubatov *et al.*,⁵ is assigned to a hyperfine satellite caused by a carbon nearest to boron. This is the largest hf interaction found for boron centers, and it has been regarded as evidence that boron substitutes for a silicon.⁵ The ^{13}C hyperfine lines can clearly be recognized in Fig. 5, where spectra are presented in a wider range of the magnetic field and on an enlarged scale. In Fig. 6, the orientational dependence of the hf splitting with ^{13}C is shown. Circles represent the hf splitting of center B_3 , and triangles are averages of those of centers B_1 and B_2 . As the lines are broad and the peaks of B_1 and B_2 are close to each other, we could not distinguish between B_1 and B_2 . For B_1 and B_2 the lines could not be followed when the

magnetic field is more than 20° away from the principal g_z axis due to a strong overlap of lines for the centers with different orientation. As for B_3 the lines could not be resolved from the main peak when the magnetic field is more than 70° away from its principal axis. The solid curve is a fitting curve $[a + b(3\cos^2\theta - 1)]$, with $a=(40.8\pm 0.5)\times 10^{-4}$ T and $b=(10.8\pm 0.5)\times 10^{-4}$ T. Here a is the isotropic and b the anisotropic hf constant. These parameters are in rough agreement with values reported by Zubatov *et al.*,⁵ which are given in Cartesian coordinates and equivalent to $a=(32\pm 1)\times 10^{-4}$ T and $b=(14.8\pm 1)\times 10^{-4}$ T. The important point is that the axial symmetry axis of the hf tensor of ^{13}C coincides with the direction of the g_z axis for all three centers. Though the absolute signs of a and b cannot be determined from this orientational dependence, their relative sign must be the same. Moreover, from the mere size of the isotropic hf interaction we can safely conclude that there is direct spin-density on carbon and hence that the a and b parameters are positive. Polarization effects, which might lead to a negative value of a , normally are responsible for at least orders-of-magnitude smaller hf interactions.

There are two important points to note concerning the g tensors. The first is that we have demonstrated that for all three centers the smallest g -values are related to g_z , and that they are very close to the free-electron g value of 2.0023. The second is that for all three centers the directions of the g_z axes coincide with the axial symmetry axes of the hf tensors (A_{zz}) of the ^{13}C nuclei.

B. Assignment of the three centers to the three sites in 6H-SiC

In 6H-SiC, there are three inequivalent lattice sites for silicon and carbon. One site, indicated as hex in Fig. 7, has a surrounding with hexagonal symmetry around the c axis and the other two, k_1 and k_2 , have quasicubic ones. From the fact that the largest hf splitting is observed for ^{13}C , it is reasonable to consider that the boron impurity is substituting for silicon.⁵ We tentatively attribute the signal B_3 to the hexagonal site and B_1 and B_2 to the two quasicubic sites. As for the assignment of B_1 and B_2 to the two quasicubic sites, we are tempted to assign B_1 with the smaller difference between g_x and g_y to the site closer to the hexagonal site, i.e., the k_1 site, and hence B_2 to the k_2 site. Later on, we will present data of the spin relaxation rates which will support this assignment. In the following, for easiness of reading, we will indicate the three centers as $B_1(k_1)$, $B_2(k_2)$, and B_3 (hex).

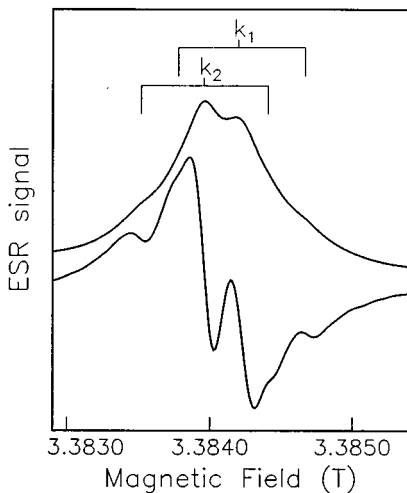


FIG. 4. The derivative of the high-field part of the EPR spectrum with $\theta=90^\circ$ and $\phi=30^\circ$. The hf components of sites k_1 and k_2 are indicated.

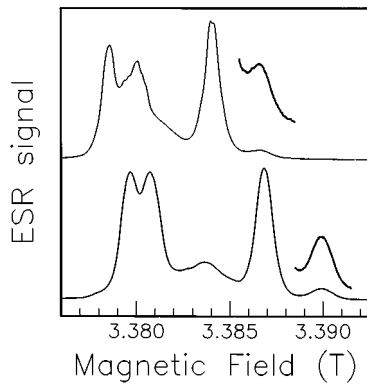


FIG. 5. The EPR spectra of the ^{13}C -enriched 6H-SiC:B sample. The upper spectrum corresponds to the orientation $\theta=90^\circ$, $\varphi=30^\circ$, and the lower spectrum to $\theta=0$ (see Fig. 3). The ^{13}C hf satellites are shown on an increased scale.

C. ENDOR of ^{11}B

ENDOR measurements of ^{11}B ($I=\frac{3}{2}$) were performed for the three centers B_1 (k_1), B_2 (k_2), and B_3 (hex). The parameters determined in the present study are almost in agreement with the parameters of Refs. 10 and 13. Some discrepancies, however, were found in the assignment of the signals to the three centers and in the data treatment. Thus, a short description of the results is given here, mainly for the B_2 (k_2) center, for which the most extensive measurements were done.

In Fig. 8 the orientational dependence of the ^{11}B ENDOR signals for the B_2 (k_2) centers is shown in a plane which contains the g_z and g_y axes. The angle θ' is the angle between the direction of the magnetic field and the g_z axis. Open and filled circles indicate the ENDOR lines which originate in the two different m_s manifolds (as yet such an assignment is not possible, but in the following discussion it will be shown that the open circles correspond to the $m_s=+\frac{1}{2}$ level). The curves in Fig. 8, which are symmetric around $\theta'=0$, show that the orientation of the principal axis of the hf tensor and the quadrupole tensor coincide with the direction of the g_z axis. This was confirmed to be the case for all three centers. Measurements in the g_x-g_y plane were also performed and the deviation from axial symmetry for the anisotropic hf and Q tensor were estimated to be $A_{xx}-A_{yy}<0.24$ MHz and $Q_{yy}-Q_{xx}<20$ kHz for B_2 (k_2) and $A_{yy}-A_{xx}<0.24$

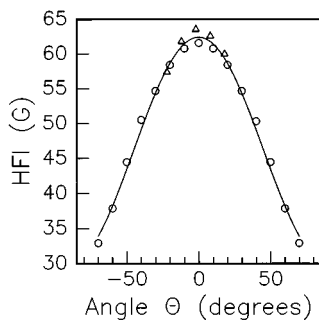


FIG. 6. The orientational dependence of the ^{13}C hf interactions of the hexagonal site B_3 (open circles). The triangles give the same orientational dependence for the quasicubic sites B_1 and B_2 as a function of the angle between the magnetic field and their g_z axis.

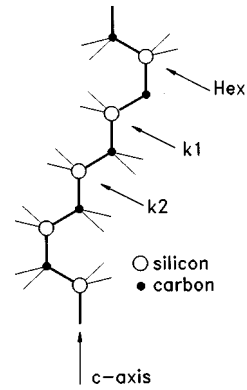


FIG. 7. The crystal structure of 6H-SiC with the positions of the hexagonal (hex) and quasicubic sites k_1 and k_2 for silicon.

MHz and $Q_{xx}-Q_{yy}<10$ kHz for B_1 (k_1). No deviation from axial symmetry was found for B_3 hex. Due to the quadrupole interaction of ^{11}B ($I=\frac{3}{2}$), three ENDOR lines are observed for each m_s manifold. The nuclear Zeeman frequency ν_z for ^{11}B depends on θ' , and is in the range 46.16–46.24 MHz, depending on the magnitude of the magnetic field at which the signal is observed. Solid and broken curves represent the theoretical fit for both m_s manifolds, taking into account the shift of $\nu_z(^{11}\text{B})$ mentioned above. The fitting parameters are listed in Table II, where the data for B_1 (k_1) and B_3 (hex) are also included. The parameters are very close to those reported in Refs. 10 and 13, but the assignment of the hf interaction constants to centers with specific g values is differ-

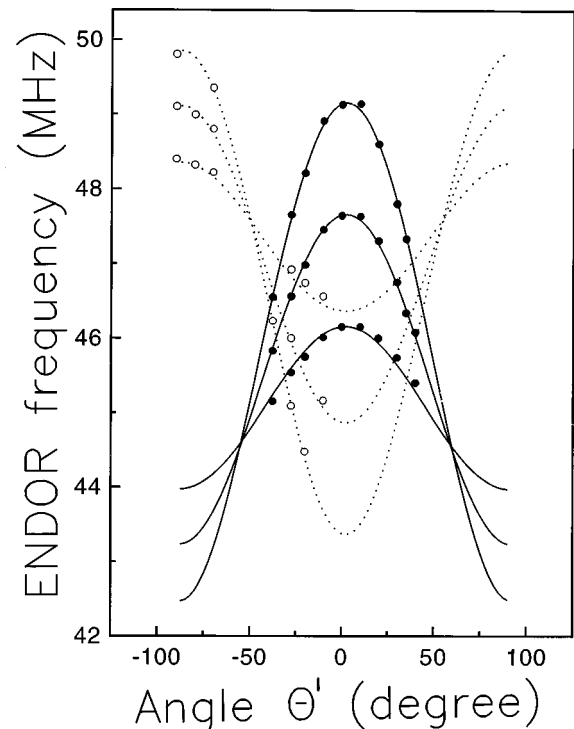


FIG. 8. The orientational dependence of the ^{11}B ENDOR signal for the B_2 (k_2) center. The black dots and open circles are experimental data, and the solid and dotted lines theoretical curves. The open circles correspond to the $m_s=\frac{1}{2}$ and the black dots to the $m_s=-\frac{1}{2}$ manifold.

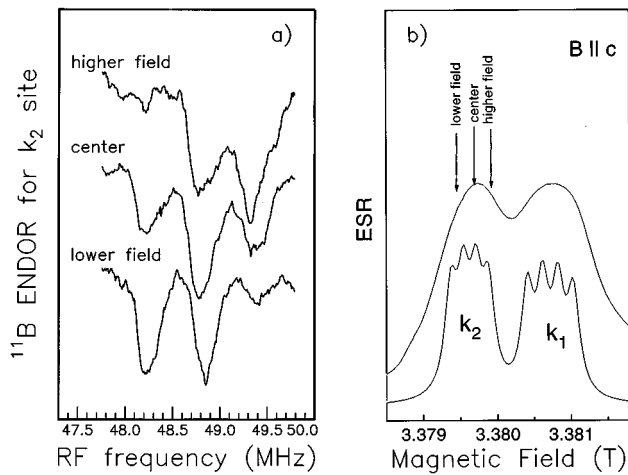


FIG. 9. (a) The ENDOR spectra of ^{11}B ($I=\frac{3}{2}$) above the Zeeman frequency recorded at different positions of the EPR line as indicated in (b). (b) The upper curve is the experimental EPR spectrum of sites k_1 and k_2 for $\mathbf{B} \parallel \mathbf{c}$ ($\theta=0$). The lower curve is a calculated spectrum showing the ^{11}B hf splitting.

ent. By measuring the ENDOR spectra for the best-resolved EPR line, it was found that the B_1 (k_1) center with the middle g_z value has the largest isotropic hf constant a , and that the B_2 (k_2) center with the largest g_z value has the middle a value. In Ref. 13, however, the largest a is assigned to k_2 with the largest g_z (g_x in their table) value, and the middle a is assigned to k_1 with the middle g_z . It is not clear how these authors assigned a specific set of hf constants to a center with a particular set of g values.

Contrary to the case of the ^{13}C hf splitting the a and b for ^{11}B have opposite sign. This fact has been found for the B_3 (hex) center by Woodbury and Ludwig,¹ for centers in 3C-SiC by Baran *et al.*,¹¹ and for B_1 (k_1) and B_2 (k_2) centers by Muller *et al.*³ The angular dependence of the ENDOR spectra gives us only the relative sign of a and b . The signs in Table II have been derived from field-tagged ENDOR measurements which give the relative sign of the hf and quadrupole interaction. The results of these experiments are presented in Fig. 9(a). Here the ENDOR spectra above the Zeeman frequency of the k_2 site are shown for $\mathbf{B} \parallel \mathbf{c}$ ($\theta=0^\circ$) for three slightly different magnetic-field positions as indicated in Fig. 9(b). In order to indicate explicitly the hf splitting of ^{11}B , the linewidth for the calculated spectrum was taken to be narrower than that for the simulations in Fig. 3. When the ENDOR experiment is performed at the high-magnetic-field side of the EPR line, the ENDOR line at the higher rf frequency is larger, as can be seen in the upper spectrum in Fig. 9(a). When observing at lower magnetic field, the lower-frequency ENDOR line is larger as shown in the lower spectrum. This indicates that the sign of the quadrupole interaction Q is the same as that of the hf interaction A .

To illustrate how the relative signs of A and Q are obtained, in Fig. 10 we present the energy-level scheme of the $S=\frac{1}{2}$, $I=\frac{3}{2}$ manifold taking the following interaction energies into account. First the electron Zeeman energy $g\beta\mathbf{B}\cdot\mathbf{S}$, second the nuclear Zeeman energy $-g_n\mathbf{B}\cdot\mathbf{I}$ ($g_n>0$ for ^{11}B), third the hf interaction energy $A\mathbf{S}\cdot\mathbf{I}$ ($A<0$), and fourth the quadrupole coupling energy $\frac{1}{2}(3m_I^2 - I(I+1))Q$. The dotted

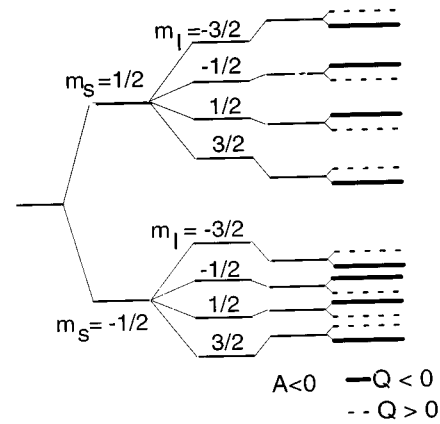


FIG. 10. The energy-level scheme of the $S=\frac{1}{2}$ electron spin and $I=\frac{3}{2}$ nuclear spin (^{11}B) system. The hf interaction A is taken to be negative, and the quadrupole interaction q negative (thick lines) or positive (thin lines).

lines reflect the situation for $Q>0$ and the thick solid lines that for $Q<0$. The level diagram with the thick solid lines are in agreement with the experimental results, as can be seen as follows. When saturating the EPR signal at the higher magnetic field, corresponding to the transition $m_S = -\frac{1}{2} \leftrightarrow +\frac{1}{2}$, $m_I = \frac{3}{2}$, the associated ENDOR transition above the Zeeman frequency ($m_S = \frac{1}{2}$, $m_I = \frac{3}{2} \leftrightarrow \frac{1}{2}$) should be stronger, and should occur at the highest ENDOR frequency. In the same way, the EPR signal at lower magnetic field brings about the lower frequency ENDOR signal. The dotted energy-level scheme for $Q>0$ will give the opposite result. It can be easily checked that the combination $A>0$, $Q>0$ will give an energy-level diagram that is also consistent with the experimental results. Thus, it is concluded from this field-tagged ENDOR that A and Q have the same sign.

The relative signs of a , b and the quadrupole constant q can now be determined using the results obtained so far. Here we take into account the following

(i) a and b have opposite sign.

(ii) $A = a + b(3 \cos^2 \theta' - 1)$ and $Q = q(3 \cos^2 \theta' - 1)$ have the same sign. Here θ' is the angle between the magnetic field and the principal z axis of the A and Q tensors, and is 110° for this case.

(iii) The angular factor $(3 \cos^2 \theta' - 1)$ is negative ($-\frac{2}{3}$) for $\theta' = 110^\circ$.

From (i) and (iii), it is concluded that the sign of A is the same as that of a . From this and (ii), it follows that Q has the same sign as a , and by taking (iii) into account that q and a have opposite signs. Thus the signs of the hf and quadrupole parameters are either $a<0$, $b>0$, and $q>0$, or $a>0$, $b<0$, and $q<0$. As q is expected to be positive, as will be discussed in Sec. IV A, we choose $a<0$, $b>0$, and $q>0$ in Table II. We repeated the field-tagged ENDOR experiments for several other orientations and sites, and they always gave the same relative sign of a , b , and q .

D. ENDOR of ^{13}C and ^{29}Si

ENDOR experiments were also performed in the range including the Zeeman frequencies of ^{13}C ($\nu_Z(^{13}\text{C}) \sim 36.2$ MHz) and ^{29}Si ($\nu_Z(^{29}\text{Si}) \sim 28.6$ MHz). In Fig. 11(a) the

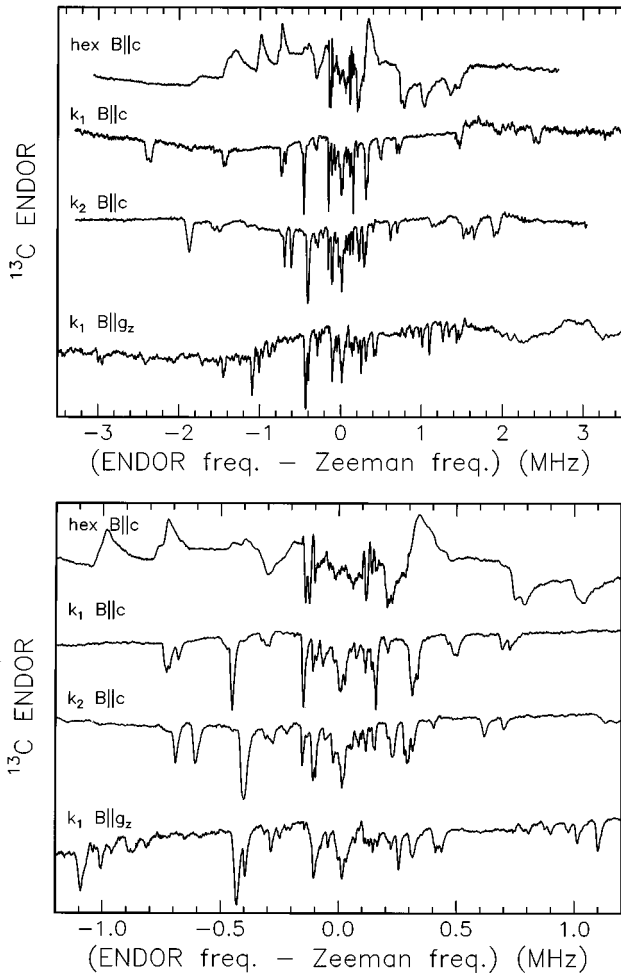


FIG. 11. The ENDOR spectra for ^{13}C on two different frequency scales. The orientation of the magnetic field is indicated in the figure.

ENDOR spectra around $\nu_Z(^{13}\text{C})$ are shown for the three centers with $\mathbf{B}||c$, and the spectrum for the $B_1(k_1)$ site with $\mathbf{B}||g_z$. The same spectra are shown on an expanded frequency scale in Fig. 11(b). In Figs. 12(a) and 12(b) the ENDOR spectra around $\nu_Z(^{29}\text{Si})$ are shown in the same manner. Each spectrum is composed of many spectra measured with different interval times τ , in order to avoid blind spot effects.²⁰ Normally, pulsed ENDOR signals appear as a decrease of the electron-spin-echo (ESE) signal, however, some lines here were found to correspond to an increase. This “positive ENDOR effect” is sometimes observed at 95 GHz, although the origin is not yet clear. One usually expects the ENDOR spectra to be symmetric around ν_Z . However, due to the “positive ENDOR effect” and also due to different intensities of lines above and below ν_Z , the ENDOR spectra, especially for ^{29}Si , do not look symmetric. As the ENDOR effect was small and it took a long time to measure spectra for one orientation, we did not perform a full orientational study. Nevertheless some conclusions can be drawn from the ENDOR spectra of Figs. 11 and 12. First, the spread in frequency for carbon and silicon is almost the same. Second, the large number of lines and their position around ν_Z indicate that a considerable spin density is present on the remote nuclei in the crystal. Third, the spread and the

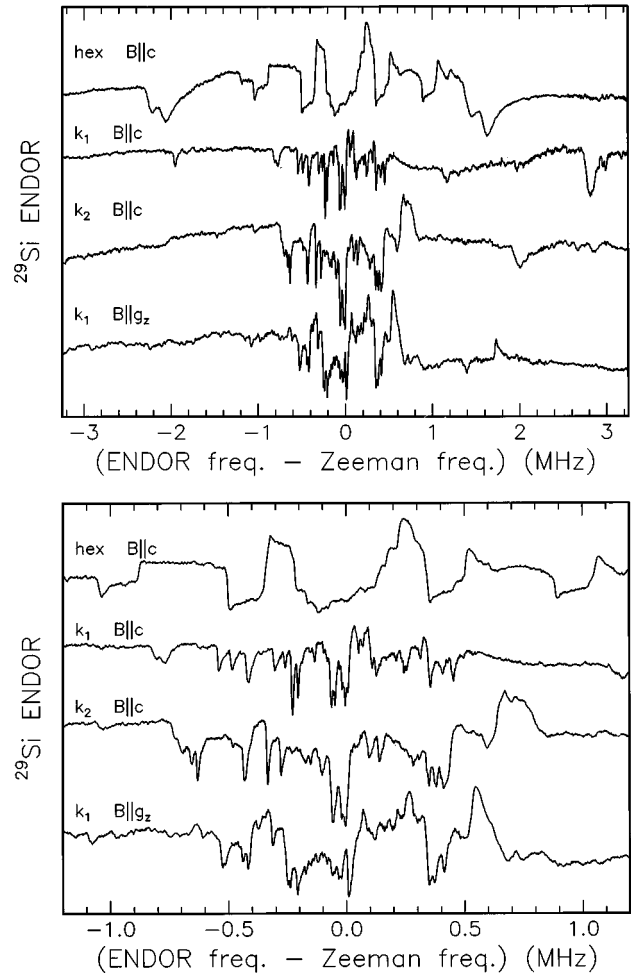


FIG. 12. The ENDOR spectra for ^{29}Si on two different frequency scales. The orientation of the magnetic field is indicated in the figure.

positions of the ENDOR lines close to ν_Z , for different orientations and for different centers are similar, which means that the anisotropic hf interaction for these nuclei is small compared to the isotropic one. This was confirmed by an orientational study of the group of ENDOR lines of ^{13}C about 1.2 MHz away from $\nu_Z(^{13}\text{C})$. The maximum shift of these lines as a function of orientation was estimated to be 0.5 MHz. This should be compared with the isotropic hf interaction for these nuclei of the order of 2.4 MHz. These facts indicate that the spin density on the remote nuclei is almost isotropic (as for the three silicon atoms nearest to the carbon carrying the main spin density) almost equally distributed between carbon and silicon atoms, and smoothly decaying when going away from the center.

E. Temperature dependence of the EPR spectra

In Fig. 13 the temperature dependence of the ESE-detected EPR spectra for $\mathbf{B}||c$ is shown. The high-field signal originates from $B_3(\text{hex})$ and the doublets seen at low field are related to the $B_1(k_1)$ and $B_2(k_2)$ centers. When the temperature is raised, the signal of the $B_2(k_2)$ center, at the lowest field, starts to decrease, followed by a decrease of the $B_1(k_1)$ signal. At 47 K the intensities of the $B_2(k_2)$ and $B_1(k_1)$

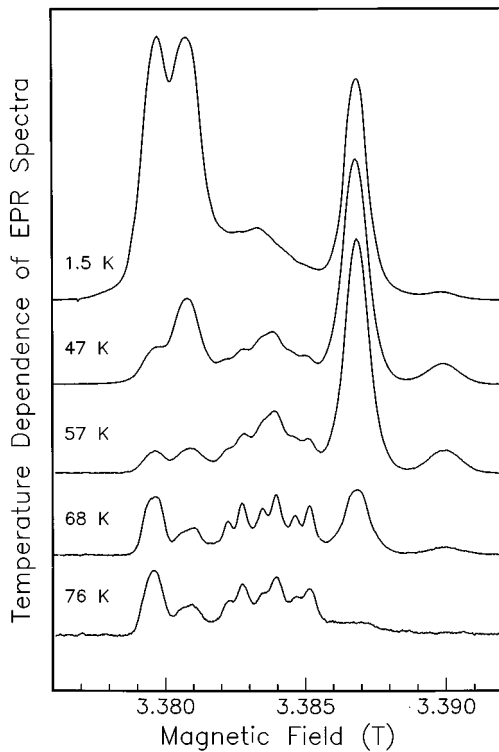


FIG. 13. The temperature dependence of the ESE detected EPR spectra for $\mathbf{B}\parallel c$.

(k_1) centers relative to that of B_3 (hex) are about 10% and 30% of the value at 1.5 K, respectively. Simultaneously the ^{13}C hf line observed around 3.390 T for the B_3 (hex) center increases considerably. These high-temperature spectra with their pronounced hf components were also used for measuring the ^{13}C hf splitting as displayed in Fig. 5. A signal around 3.384 T is due to the N donor. At 57 K this feature increases further. The signal of the B_3 (hex) center starts to decrease at 68 K, when the B_2 (k_2) center starts to grow. At 76 K the signal of the B_3 (hex) center has completely disappeared. At temperatures higher than 57 K, signals from B_1 (k_1) and B_2 (k_2) centers can be observed only for the orientation $\mathbf{B}\parallel c$. The temperature dependence of the spin-spin relaxation time T_2 , as measured in a two-pulse echo experiment for the three sites, is shown in Fig. 14.

IV. DISCUSSION

A. Electronic structure of the shallow boron acceptor

Here we discuss a model for the electronic structure of the boron center which can consistently explain all our experimental observations. We observe, first, that the g tensors are axial or almost axial for all three centers, with g_z closest to the free-electron value and with g_x, g_y at slightly larger values. Second, the two components a and b of the hf interaction with ^{13}C have the same sign. Third, the hf interaction and quadrupole interaction with ^{11}B and is given by $a < 0$, $|a| < 4$ MHz, $b \sim 3$ MHz, and $q \sim 250$ kHz. Fourth, that the directions of the axial z axis of the g tensor, the hf tensor for ^{13}C and the hf and quadrupole tensors for ^{11}B are the same, and along the c axis for B_3 (hex) and 70° away from the c axis for B_1 (k_1) and B_2 (k_2).

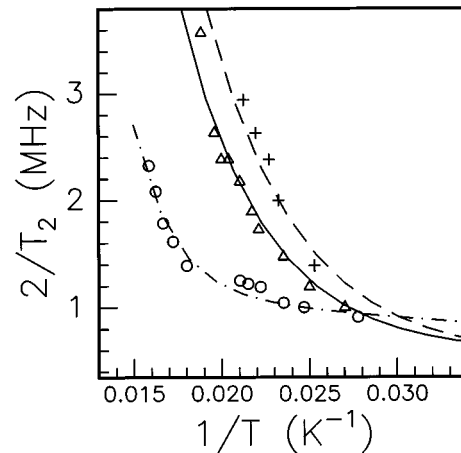


FIG. 14. The variations of the spin-spin relaxation rate $1/T_2$ as a function of the inverse temperature. The open circles apply to B_3 (hex), the triangles to B_1 (k_1), and the crosses to B_2 (k_2).

As we have seen, the largest hf interaction is observed with ^{13}C . A reasonable assumption is that this carbon atom, which carries the highest spin density, is the one nearest to boron, which occupies a silicon position. For symmetry reasons the common axial direction for all magnetic-resonance parameters for this center should be along this C-B bond. For B_3 (hex), this bond is along the c axis, and for B_1 (k_1) and B_2 (k_2), along a direction 70° away from c .

In our model, the unpaired spin density is mainly localized on the p_z orbital of a carbon which is nearest to boron, i.e., along the c axis for B_3 (hex) and 70° away from the c axis for the B_1 (k_1) and B_2 (k_2) sites. This p_z orbital is directed along the C-B connection line, and the C-B bond is a dangling bond. Boron is neutral and carries no direct spin density. There is a relaxation of the carbon atom, which carries spin density, and the boron atom, which move away from each other. We will show in the following that this model is consistent with all experimental observations.

According to our model, there is a direct spin density on the p_z orbital of the carbon nearest to boron. This means that the hf tensor of the ^{13}C nuclear spin should be axially symmetric along this p_z orbital, i.e., along the C-B connection line, and that the sign of b and, hence, of a , should be positive in agreement with the experimental results. If we make a simple estimate of the spin density on the carbon atom from a and b , as was done in (Ref. 5) by assuming that the atomic orbital of carbon in SiC does not differ from that of a free carbon atom, we find 3% s character and 27% p character.²¹ As a consequence the fraction of p character, $27\%/(3+27\%) = 0.9$, and thus is larger than 0.75, as expected for a sp^3 hybrid orbital. This suggests that the four orbitals of carbon are shifted from sp^3 hybrid orbitals to three sp^2 hybrid orbitals and one pure p orbital, in which the unpaired spin is mainly localized. This means that the carbon atom is relaxed away from boron. If we assume that carbon is in a $sp^2 + p$ configuration, then the 3% spin density in the s orbital should be shared between three sp^2 orbitals. This results in three sp^2 orbitals, with 1% density in the s orbital and 2% in the p orbital. The spin density in orbitals which are perpendicular to the principal axis of the hf interaction makes a negative contribution to the anisotropic hf constant b . In order to obtain the experimental b value, the spin density in the

p_z orbital should be increased to 29% to cancel this negative contribution. In total, without taking into account polarization effects, the spin density at the nearest carbon is estimated to be $3(1+2)+29=38\%$.

We note that according to the ‘‘boron-induced carbon-acceptor’’ model,¹³ which locates the unpaired spin on three C-Si bonds 109.47° away from the B-C bond, the sign of b along the B-C bond should be negative. In addition, in order to explain the observed value of $b \approx 3$ MHz for B, we have to assume almost 100% of the spin density on these three sp^3 hybrid orbitals of the nearest carbon. This is in contradiction to our ENDOR data, which clearly demonstrate a substantial delocalization of the spin density on the remote nuclei. Moreover, with this model, one should expect a huge value for the hyperfine interaction a , for ¹³C, as the spin density is localized on sp^3 hybrid orbitals. Note that only 3% spin density in the s orbital is sufficient to give $a \sim 40 \times 10^{-4}$ T.

The deviation of the carbon orbitals from a sp^3 hybrid configuration to a sp^2 configuration indicates the presence of a shift of the carbon atom from its central position away from boron along the C-B connection line. We believe that the same shift happens for boron as the covalent radius of boron is smaller than that for silicon,⁹ and since there is no bond between carbon and boron. Moreover a quantum-chemical calculation for cubic SiC¹² (Ref. 12) confirms the relaxation of boron and carbon away from each other.

As concerns the g tensor, the finding that the deviation of g_z from g_e is zero further supports our model in which the unpaired electron is localized in the p_z orbital because the expectation value of the orbital angular momentum along this direction is zero.²²

With regard to the hyperfine interaction with ¹¹B there is no direct spin density on boron in our model, and, consequently, the anisotropic part of the hf interaction is determined by the dipole-dipole interaction with the unpaired spin in the p_z orbital of carbon. Here we will show that this dipole-dipole interaction can explain the sign and order of magnitude of the experimentally observed hf parameters. First of all, the sign of the hf constant b is predicted to be positive, and the hf tensor is axially symmetric with the symmetry axis along the dangling bond, in agreement with the experimental data. To estimate the value of b , we use a point-dipole approximation. To account for the 3% spin density in the s orbital, we put $0.03(-e)$ at $r=1.89$ Å (the Si-C distance in the perfect crystal) from boron, and, to account for the 27% of spin density in the p orbital parallel to the B-C bond, $0.27/2(-e)$ at $r-0.77$ Å and $r+0.77$ Å. The value of 0.77 Å has been taken from Ref. 23. This estimate gives $b=+2.7$ MHz, in good agreement with the observed value of about +3 MHz. A more realistic calculation should use Slater-type atomic orbitals for the distribution of the spin density, but as the radius of the p function is not known (especially not in the SiC crystal), we applied the simplest form of the approximation.

The isotropic part of the boron hf interaction is very small and negative. Here we have to realize that only 0.1% of the spin density in the s orbital of boron gives $a \sim 3$ MHz. This indicates that there is a subtle balance between different types of polarization effects which are responsible for the value of a , as was noticed in Ref. 16. This is consistent with our proposed model, in which there is no direct spin density

on boron. In fact, the value of a is the only parameter which differs considerably between the B₃ (hex) and quasicubic [B₁ (k_1) and B₂ (k_2) centers (see Table II)]. Qualitatively, polarization effects might be understood on a semiempirical level for simple organic radicals,²⁴ but, for crystals, the situation is much more complicated. Our feeling is that there is no theoretical basis for even a simple speculation on the sign and the value of a for boron.

The quadrupole tensor of ¹¹B is determined by two main contributions. One is the electric-field gradient (EFG) produced by the distribution of the electrons in the four orbitals of boron and the other is the EFG produced by the spin density on the p_z orbital of C. Both these contributions are expected to be positive. The latter one can be estimated from the anisotropic hf parameter b by the expression

$$q = \frac{b}{2I(2I-1)} \frac{e^2 Q}{\mu_\beta \mu_n g_n} (1-\gamma), \quad (1)$$

where Q is the electric quadrupole moment of ¹¹B, and $(1-\gamma)$ is the Sternheimer antishielding factor. Taking $b=+3$ MHz, q is estimated to be +27 kHz without taking into account the antishielding factor, which is supposed to be not very effective for crystals with strong covalent bonds. Since the carbon atom is slightly positively charged, since there is only 27% of spin density in the p_z orbital, this contribution is positive but too small to explain the experimental value of +250 kHz.

Next, we estimate the contribution from the three valence electrons in the orbitals of boron. The experimental value of $eQV_{zz,0}$ for the ¹¹B atom produced by one p electron is -5.39 MHz,²⁵ where $V_{zz,0}$ is the EFG for an atom. For boron with hybrid orbitals,

$$\frac{eQV_{zzz}}{eQV_{zz,0}} = \frac{-3 \cos\beta}{1 - \cos\beta} (l-m), \quad (2)$$

where β is the angle between the C-Si bonds, l is the population of the orbital along z , and m the population of the other three orbitals.²⁶ For sp^3 hybrid orbitals β is 109.47° and $-3 \cos\beta/(1-\cos\beta)=3/4$. As this is a rough estimation, we did not take into account the displacement of boron, which makes the orbitals closer to sp^2 hybrids, for which $\beta=120^\circ$ and this factor is -1 . The experimental value q is defined as $q=eQV_{zzz}/(4I(2I-1))$ with $I=3/2$ for ¹¹B. Thus the value of q for ¹¹B with a sp^3 configuration, with no electron present in the bond along z ($l=0, m=1$), is $q=-5.39 \text{ MHz} \times \frac{3}{4} \times (0-1)/12 \sim +340$ kHz. This value is in reasonable agreement with our experimental value, $q=+250$ kHz, especially when we take into account that the radius of the p functions in a crystal with a high dielectric constant can be larger than that of an atom, which makes $V_{zz} (\propto \langle r^{-3} \rangle)$ and hence q smaller.

B. Spin distribution in the crystal

In the previous sections, we established that the spin density on the central carbon is around 38%, and negligible on boron. We can make a similar estimate for the three silicon neighbors of the carbon by considering the shf interaction with ²⁹Si. The observed isotropic a parameter of 10×10^{-4} T corresponds to a spin density of 0.6% on the s orbital of

silicon. If we assume sp^3 hybrid orbitals for silicon, the total spin density on silicon is supposed to be four times larger, i.e., 2.4%. The small anisotropic b parameter of less than 2.8 MHz can be partly ascribed to the 38% spin density on the carbon, whose contribution is estimated to be between 0.6 and 0.9 MHz from a point-dipole approximation. The rest is considered to be due to an anisotropic spin distribution among the four sp^3 bonds. For instance, a population difference between one Si-C bond and the other three of 0.9% adds 1 MHz to b . We thus estimate 1.5% (1.125% p character) spin density on the Si-C bond and 0.3% (0.225% p character) on the others. In total the spin density on carbon and the three silicon neighbours of carbon sums up to 45%.

For the more remote nuclei, we have to inspect the ENDOR spectra for ^{13}C and ^{29}Si . Since the orientational dependence of the ENDOR spectra was not available, we could not attribute the ENDOR lines to a specific nucleus. In the following, we will make a rough assignment of the ENDOR lines to shells of nuclei and estimate the spin distribution. The shells are defined as groups of nuclei which are at a given distance from the carbon atom which carries the highest spin density.

In the ENDOR spectra, the signals far away from the Zeeman frequency correspond to a large hf interaction A , and are supposed to be from nuclei which are closest to the center of the spin distribution. We assume that the center of the spin density distribution is located on carbon, judging from its large spin density. An interesting point to note is that this carbon atom, for boron centers substituting for silicons at the hexagonal as well as the k_1 site, has hexagonal symmetry, whereas for the k_2 site this carbon has quasicubic symmetry. The number of nuclei in a particular shell is, in principle, different for the hexagonal site and the k_2 site. In the discussion hereafter, the number of nuclei in a shell corresponds with that for the hexagonal carbon.

The outermost group of lines in the ^{13}C ENDOR spectrum is observed around 2 MHz. We assign these lines to the carbons that are the nearest neighbors to silicon next to the central carbon. We call these nine carbons the second-shell carbons. We exclude the three carbons next to boron, which in principle also belong to this shell, because the spin density on boron is negligible. From a similar analysis as the one applied to ^{29}Si , a spin density of 0.4% is expected for each of the nine carbons from the second shell. As for the ^{29}Si ENDOR, the outermost line around 3 MHz is ascribed in the same way to the 12 silicons in the third shell, of which each nucleus carries 0.5% spin density. In the ^{13}C spectrum the group of lines around 1 MHz is tentatively assigned to the fourth and sixth carbon shells, which include six and 24 carbons, respectively. The average spin density on each nucleus in these shells is estimated to be 0.2%. A similar group of lines in the ^{29}Si spectrum around 1.5 MHz is assigned to the fifth and seventh shells with 12 and 16 silicons, of which each spin carries an estimated spin density of 0.26%. The group of lines around the nuclear Zeeman frequency is ascribed to farther ^{29}Si and ^{13}C nuclei. The average spin density on these silicon and carbon nuclei is estimated from the average separation of these ENDOR lines from the Zeeman frequency to be 0.05%. We assume that about 100 carbon and 100 silicon nuclei are involved. We thus find a total spin density of 33% on the remote nuclei.

As can be seen in Figs. 11 and 12 the ENDOR spectra of silicon and carbon show a similar pattern with a similar separation of the ENDOR lines from the nuclear Zeeman frequency. This indicates that the distribution of the spin density does not depend on the kind of nucleus, and that it is quite smoothly delocalized in the crystal, especially for the far-away nuclei. Assuming effective-mass theory (EMT) to be valid, we expect that the decay of the spin density is exponential from the third shell (0.5% spin density) onwards. The spin density distribution close to the center deviates from this hydrogenlike distribution and is anisotropic, as there is almost no spin density on boron. Since about 50% of the spin density is within the first two shells about 50% obeys this exponential decay with distance r . With the restriction that the sum of the spin densities on the nuclei from the third shell to infinity is equal to 50%, for the Bohr radius we obtain $r_0 = 2.2 \text{ \AA}$. It is interesting to note that from EMT, using for the ionization energy the value 0.3–0.39 eV and for the dielectric constant the value 6.5–10, a Bohr radius r_0 between 2 and 3 \AA is predicted. It is seen that the value of r_0 estimated from the ENDOR data is in reasonable agreement with this theoretically predicted Bohr radius.

C. Temperature dependence of the EPR spectra

Finally we discuss the temperature dependence of the EPR spectra, which reveals the electronic structure of the centers at high temperatures. This temperature dependence is consistent with the previous observations.⁵ When increasing the temperature the dangling bonds of the $B_1(k_1)$ and $B_2(k_2)$ centers start to jump between the three equivalent carbon atoms in the plane perpendicular to the c axis. When further increasing the temperature, the jumping involves all four neighboring carbon atoms. For the hexagonal site the jumping starts at higher temperatures than for the quasicubic sites, and it involves all four neighboring carbon atoms.

The jump rate determines the spin-spin relaxation time T_2 . When increasing the temperature the jump rate goes up and the T_2 time shortens, leading to the disappearance of the ESE-detected EPR spectra. The jumping between the three equivalent carbon atoms in the plane perpendicular to the c -axis does not affect the EPR spectra of sites $B_1(k_1)$ and $B_2(k_2)$ when the magnetic field is parallel to the c axis. This is the reason that field-swept ESE spectra for these centers can still be seen for this orientation up to 90 K. At temperatures higher than 90 K the dangling bond of the $B_1(k_1)$ and $B_2(k_2)$ centers start to jump between all four carbon atoms, and the EPR spectra disappear for all orientations.

As the T_2 time at high temperatures is determined by the jump rate, the activation energy for this process can be determined from the temperature dependence of T_2^{-1} as shown in Fig. 14. At temperatures above 40 K, T_2^{-1} has the largest value for $B_3(\text{hex})$ and the smallest for $B_2(k_2)$. The activation energy for the increase of T_2^{-1} was estimated using the expression $1/T_2 = 1/\tau + \nu \exp(-\Delta E/kT)$. For the $B_1(k_1)$ and $B_2(k_2)$ centers a value $\Delta E = 20 \text{ meV}$ is found, and for $B_3(\text{hex})$ $\Delta E = 40 \text{ meV}$.

At the lowest temperature of $\sim 1.2 \text{ K}$, the T_2 of $B_2(k_2)$ was found to be about $12.2 \pm 0.5 \mu\text{s}$ as compared to $6.0 \pm 0.2 \mu\text{s}$ for $B_3(\text{hex})$ and $B_1(k_1)$. This is an important observation. At low temperatures, T_2 is determined by the dipole-dipole interactions of the electron spin with the surroundings nuclei.

From our experiment we conclude that for B_3 (hex) and B_1 (k_1) the magnetic surroundings with respect to the unpaired spin is the same. As we mentioned above, the carbon atom with the main spin density has the same position in the crystal for both the B_3 (hex) and B_1 (k_1) centers, and hence has the same surroundings. This is the carbon atom in the hexagonal position, whereas for the B_2 (k_2) center this carbon atom is in the quasicubic position. We used this observation to confirm our assignment of the EPR signals to the two quasicubic sites k_1 and k_2 .

IV. CONCLUSIONS

The high-frequency pulsed EPR/ENDOR study at 95 GHz of the ^{13}C -enriched 6H-SiC single crystal has enabled us to present a consistent model of the electronic structure of the shallow boron acceptor center, which explains all available magnetic resonance data. The high spectral resolution and the possibility to perform a complete orientational EPR and ENDOR study play a crucial role in this investigation. The g tensors, the hf tensors of ^{13}C and ^{11}B , and the quadrupole tensors of ^{11}B for each boron site in the 6H-SiC crystal were measured and analyzed. It is concluded that around 40% of the spin density is localized in the p_z orbital of a carbon which is nearest to boron. This p_z orbital is along the c axis for the B_3 (hex) and 70° away from the c axis for the B_1 (k_1)

and B_2 (k_2) sites. The p_z orbital is directed along the C-B connection line, and the C-B bond is a dangling bond. Boron is neutral and it carries no direct spin density. There is a relaxation of the carbon atom, carrying the spin density, and the boron atom away from each other. From a ^{29}Si and ^{13}C ENDOR study it is further concluded that around 60% of the spin density is distributed in the crystal with a Bohr radius of about 2.2 Å a value that is in reasonable agreement with effective-mass theory. The measurement of the T_2 relaxation times enables the determination of the activation energies of the thermally induced dynamical averaging processes, which influence the EPR spectra at high temperatures. Moreover, the magnetic resonance parameters could be assigned to the specific quasicubic sites k_1 and k_2 .

ACKNOWLEDGMENTS

This work forms part of the research program of the "Stichting voor Fundamenteel Onderzoek der Materie" (FOM) with financial support from the "Nederlandse Organisatie voor Wetenschappelijk Onderzoek" (NWO). Further support was obtained from the Human Capital and Mobility (HCM) program of the Commission of the European Community under Contract Nos. ERBCHRXT93028 and ERBCIPDCT940612. T.M. thanks the financial support by a "Grant-in-Aid for Encouragement of Young Scientists."

-
- ¹H. H. Woodbury and G. W. Ludwig, *Phys. Rev.* **124**, 1083 (1961).
- ²M. Toyama *J. Phys. Soc. Jpn.* **20**, 1827 (1965).
- ³G. E. G. Hardeman and G. B. Gerritsen, *Phys. Lett.* **20**, 623 (1966).
- ⁴A. I. Veinger, Ya. A. Vodakov, Y. I. Kozlov, G. A. Lomakina, E. N. Mokhov, V. G. Oding, and V. I. Sokolov, *Pis'ma Zh. Tekh. Fiz.* **6**, 1319 (1980) [*Sov. Tech. Phys. Lett.* **6**, 566 (1980)].
- ⁵A. G. Zubatov, I. M. Zaritskii, S. N. Lukin, E. N. Mokhov and V. G. Stepanov, *Fiz. Tverd. Tela (Leningrad)* **27**, 322 (1985) [*Sov. Phys. Solid State* **27**, 197 (1985)].
- ⁶Le Si Dang, K. M. Lee, G. D. Watkins, and W. J. Choyke, *Phys. Rev. Lett.* **45**, 390 (1980).
- ⁷P. G. Baranov, V. A. Vetrov, N. G. Romanov, and V. I. Sokolov, *Fiž. Tverd. Tela (Leningrad)* **27**, 3459 (1985) [*Sov. Phys. Solid State* **27**, 2085 (1985)].
- ⁸P. G. Baranov and N. G. Romanov, *Appl. Magn. Res.* **2**, 361 (1991); *Mater. Sci. Forum* **83–87**, 1207 (1992).
- ⁹P. G. Baranov and E. N. Mokhov, *Phys. Solid State* **38**, 798 (1996); P. G. Baranov, I. V. Ilyin, and E. N. Mokhov, *Solid State Commun.* **100**, 371 (1996).
- ¹⁰T. L. Petrenko, V. V. Teslenko, and E. N. Mokhov, *Fiz. Tekh. Poloprovodn.* **26**, 1556 (1992) [*Sov. Phys. Semicond.* **26**, 874 (1992)].
- ¹¹N. P. Baran, V. Ya. Bratus', A. A. Bugai, V. S. Vikhnin, A. A. Klimov, V. M. Maksimenko, T. L. Petrenko, and V. V. Romanenko, *Phys. Solid State* **35**, 1544 (1993) and references therein.
- ¹²T. L. Petrenko, A. A. Bugai, V. G. Baryakhtar, V. V. Teslenko, and V. D. Khavryutchenko, *Semicond. Sci. Technol.* **9**, 1849 (1994).
- ¹³R. Müller, M. Feege, S. Greulich-Weber, and J.-M. Spaeth, *Semicond. Sci. Technol.* **8**, 1377 (1993).
- ¹⁴J. Reinke, R. Müller, M. Feege, S. Greulich-Weber, and J.-M. Spaeth, *Mater. Sci. Forum* **143–147**, 63 (1994).
- ¹⁵J. Reinke, S. Greulich-Weber, J.-M. Spaeth, E. N. Kalabukhova, S. N. Lukin, and E. N. Mokhov, *Inst. Phys. Conf. Ser. (UK)* **137**, 211 (1994).
- ¹⁶F. J. Adrian, S. Greulich-Weber, and J.-M. Spaeth, *Solid State Commun.* **94**, 41 (1995).
- ¹⁷Yu. A. Vodakov, E. N. Mokhov, M. G. Ramm, and A. D. Roenkov, *Krist. Technol.* **5**, 729 (1979).
- ¹⁸R. T. Weber, J. A. J. M. Disselhorst, L. J. Prevo, J. Schmidt, and W. Th. Wenckebach, *J. Magn. Res.* **81**, 129 (1989).
- ¹⁹J. A. J. M. Disselhorst, H. van der Meer, O. G. Poluektov, and J. Schmidt, *J. Magn. Res.* **115**, 183 (1995).
- ²⁰W. B. Mims, in *Electron Paramagnetic Resonance*, edited by S. Geschwindt (Plenum, New York, 1992).
- ²¹J. R. Morton and K. F. Preston, *J. Magn. Res.* **30**, 377 (1978).
- ²²N. M. Atherton, *Principles of Electron Spin Resonance* (Ellis Horwood Limited, Chichester, 1993).
- ²³W. J. Buma, E. J. J. Groenen, J. Schmidt, and R. de Beer, *J. Chem. Phys.* **91**, 6549 (1989).
- ²⁴T. Yonezawa, T. Kawamura, and H. Kato, *J. Chem. Phys.* **50**, 3482 (1969).
- ²⁵G. Wessel, *Phys. Rev.* **92**, 1581 (1953).
- ²⁶E. A. C. Lucken, *Nuclear Quadrupole Coupling Constants* (Academic, London, 1969).